Electrical Component Model for a Lithium Iron Phosphate Cell

W. A. Lynch and N. A. Sondergaard

Abstract **A lumped parameter electrical component model of a 26650 size LiFePO4 cell was developed based on charge and discharge plots at various rates. Step responses of the cell from seconds to hours were considered. An impedance element model was developed with components associated with the current collection grid, the active plate materials, and the electrolyte. Model elements may be approximated as resistors and capacitors; however some of the values of capacitor and resistor elements vary as a function of state of charge, load current, and temperature. Voltage dependant voltage sources were included in series with the bulk capacitor to model the nonlinear characteristics of the open circuit voltage at high and low states of charge. Constant current charge and discharge data were used to develop components of the open circuit voltage model and the total value of cell impedance as a function of current. Resistance components and pulse capacitance were determined using data from higher rate pulse test cycles. Charge and discharge plots at various temperatures in addition to cell temperature plots were used to develop the thermal model.**

Introduction

Lithium Ion batteries continue to be developed because of their power, energy and cycling advantages over more conventional battery chemistries such as lead acid, NiCd and nickel metal hydride. Lithium Ion batteries are themselves really a family of different combinations anode and cathode materials which can both intercalate lithium ions. The charged and discharged state of the cell results from the transfer of Li ions from the anode to the cathode within the cell while transferring electrons through an external circuit doing useful electrical work.

There are many manufacturers of Li Ion cells and they generally provide data sheets with a limited number of discharge curves typically at one temperature. It is well known that Li-Ion cells can be damaged and do damage when operated outside limits of recommended voltages and temperatures. This becomes especially important near the high temperature, high discharge rate limits which are challenging to estimate and often require extensive and expensive experimental testing. It is therefore desirable to have good models of cell behavior especially when designing battery systems with large numbers of cells.

Modeling has been done on Li-Ion batteries ranging from fundamental physics based models to simple empirical correlations. The former are useful for cell design and optimization but can be cumbersome when designing banks of cells. The latter approach is less computationally intensive but requires extensive data. An intermediate approach involves developing a model of cell behavior around standard circuit elements. The thus derived circuit elements can then be ported to conventional circuit modeling software such as P-Spice to design an optimized multi-cell system.

The most mature lithium ion batteries are based on LiCoO2 anodes and carbon cathodes which have open circuit voltages in the middle of their discharge curves of about 3.6 volts. LiCoO2 type lithium ion cells as well as the polymer varieties provide very high energy density. More recent development has focused on LiFePO4 cathodes. LiFePO4 cells feature a moderate cell voltage of about 3.2 volts and fairly high specific energy with long cycle life and improved stability compared with LiCoO2 and other lithium ion cells with metal oxide cathode materials. This translates to a higher degree of safety.

For the present study we have chosen to focus on LiFePO4 chemistry, in particular the ANR26650M1A cell. This cell has a good compromise between power and energy characteristics and there is a significant body of published data to calibrate the model [1],[2],[3].

Many groups have looked at modeling LiFePO4 batteries. Recently Prada [3] et.al discuss much of the full physics based models together with associated challenges and present in their paper a physics based model which features a current dependent radius pseudo particle. As reported the model produces good agreement with the A123 26650 experimental results for continuous discharge/charge but does not reproduce interval data although the authors report they are continuing to develop their model. Interval discharge data is important and has been the subject of recent experimental efforts developing repetitive pulsed power supplies using cells such as the 26650. [4],[5],[6]. Other authors have reported similar challenges modeling interval data. Chow et.al. report successfully reproducing continuous discharge data for the A123 26650 by fitting a multi parameter resistance expression but require using Matlab Simulink to reproduce the interval data [7]. Matlab can be used to estimate parameters in multi time constant LiFePO4 cell model [8] for simulations with interval data. A prismatic lithium ion cell was modeled using PSCAD in [9] and included a 3 RC circuit impedance model and a polynomial fit for open circuit voltage (OCV) which was used for continuous cycle simulation, but not tested for interval data.

In the present study we chose to develop the circuit element based model in spread sheet form to make it easily understood, usable for a wide variety of load and charging profiles including pulsed interval currents, while being implemented in widely accessible, inexpensive software. The circuit parameters developed can then be ported to circuit element based software such as PSpice to continue to investigate the performance of multi cell designs with variations in component parameter values that can simulate real world imbalances.

Model Development

Both deep cycle type lead acid [10] and Nickel-Cadmium [11] batteries are mature technologies used in a wide range of applications and have been previously modeled with similar techniques described herein.

The net electrochemical equation in a NiCd cell for example is the sum of the anode and cathode equations and the nominal cell voltage is the potential difference. In a NiCd cell OH- ions travel through the electrolyte, but there is no net change in the electrolyte. There is however a transient component of the model because at high rates the hydroxide can be depleted or possibly over concentrated near one of the electrode surfaces and in pores of the cell electrodes. The voltages at the electrodes of this cell are close to the edge of the aqueous electrolyte window, so when the cell is near a full state of charge (SOC) hydrogen and oxygen gasses can be evolved and these recombine inside the cell releasing heat. This is modeled as a non-linear self discharge component in parallel with the terminal voltage which can shunt excess charge current. A battery model can be applied in simulations such as [12] used for electric vehicle applications.

(1) $Cd + 2OH^- \rightarrow Cd(OH)_2 + 2e^-$ - 0.82 V

(2) $2NiOOH + 2H_2O + 2e^- \rightarrow 2Ni(OH)_2 + 2OH^-$ +0.49 V

(3) $Cd + 2NiOOH + 2H_2O \rightarrow Cd(OH)_2 + 2Ni(OH)_2$ 1.31 V

The net electrochemical equation in a lithium ion cell such as the LiCoO2 cell is also a sum of the two equations and the nominal cell voltage is the potential difference. Aprotic solutions are required to support the high operating voltage of lithium ion cells. Similarly in the case of lithium iron phosphate the negative anode voltage requires an aprotic electrolyte, however the lower voltage cathode provides a wider voltage safety margin. Unlike NiCd cells and other aqueous electrolyte types, lithium ion cells cannot accept any overcharge because reversible breakdown of the electrolyte cannot be used as an electron shuttle mechanism. In addition the self discharge rate of the lithium iron phosphate cell is very low so this can be neglected except when modeling cycles with very long time duration therefore the model currently includes no shunt impedance component.

The present $LiFePO_4$ model includes two RC circuits, one series resistor alone R_s and one parallel RC circuit R_p and C_p and a larger capacitor C_b that is in series with both resistors. The resistance components are functions of current, SOC, and temperature. The OCV model is associated with the larger capacitor. This includes multiple Voltage Controlled Voltage Source VCVS components that are used to develop an OCV model to fit test data which can be either symmetric or asymmetric.

Impedance Model Element Values

Model element values are determined from experimental battery cycle test data on the ANR26650M1A published by Reid [1] and Jeevarajan [2]et.al. The values of impedance components R_s and R_p are functions of current, temperature and V_b which is a linear function of SOC. R_s is equivalent to AC impedance in some datasheets and the sum of R_s and R_p is equivalent to DC impedance in some datasheets.

(4) $R=F(I, T, V_b) = F(I)*F(T)*F(V_b)$

The resistance value is the product of a function of current and factors that compensate for temperature and SOC. The current factor is 1 at a reference temperature of 20 deg C and the SOC factor is close to 1 at mid SOC which corresponds to 0 volts across capacitor V_b.

The battery model shown in Figure 1 includes two series impedance elements and a non-linear bulk capacitance and voltage source section that can be is modeled using a constant bulk capacitor C_b that is the maximum cell capacitance value in series with three voltage dependent voltage sources all of which are functions of Vb. These include symmetric source Vc0 and asymmetric sources Vc1 and Vc2. The shunt element included in aqueous cell models such as NiCd [11] is a relatively large resistance and is not included in this model because lithium ion cells have low self discharge rates and cannot accept overcharge. The terminal voltage, V_t is the load or battery charger voltage. I_L is the load current which is negative when the battery is being charged. R_s is the ac impedance of the cell. It can be measured automatically by some battery evaluation systems which generate a ripple current and determine the impedance by measuring the magnitude of the resulting ripple voltage. It is also specified on some manufacturer's datasheets and can be found from the instantaneous voltage drop in a transient step response plot. The RC time constant associated with impedance elements consisting of C_p and R_p and is presumed to result from a charge depletion layer on the plates and current flow constriction that may be caused by low Li+ ion concentration in electrolyte in pores of electrode active materials or excess Li+ in pores of electrode active materials. The open circuit float voltage V_f is the sum of nominal open circuit voltage V_n, the voltage across the bulk capacitance C_b and the voltages across the three VCVS elements that make the net effective capacitance become nonlinear.

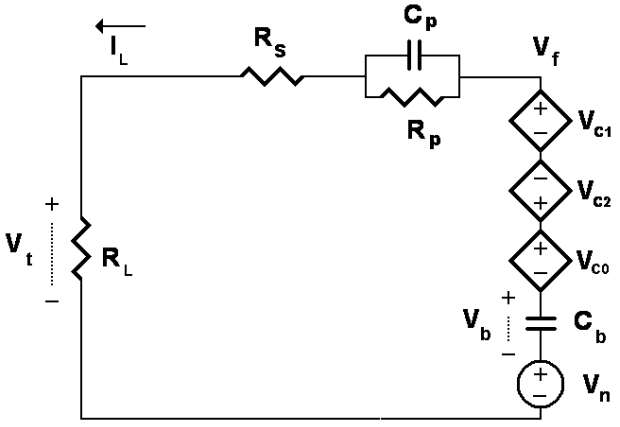

Figure 1 Component Lithium Ion Cell Model

Projections of the impedance at various test current levels based on [1] are plotted in Figure 2. This value is a function of current, however at high rates it is fairly close to 25 milli-ohms near 50% SOC and 25 deg C. At low current rates it has a non-linear characteristic similar to two anti-parallel diodes.

(5) $F(I)=R_b*(1+K_g*(Abs(I_L)+K_y)^{K_z}+R_{bd}*$ Discharge State
(6) $F_s(I)=R_{bs}*(1+K_{gs}*(Abs(IL)+K_{ys})^{K_{zs}}+R_{bd}*SIGN(-I_L)+1)/2$
(7) $F_p(I)=R_{bp}*(1+K_{gp}*(Abs(IL)+K_{yp})^{K_{zp}}$
where $R_{bs}=5$, $R_{bp}=16$, $R_{bd}=8$, $K_{gs}=8$, $K_{ys}=1$, $K_{zs}=-2$ $K_{gp}=1$, $K_{yp}=1$, $K_{zp}=-1$

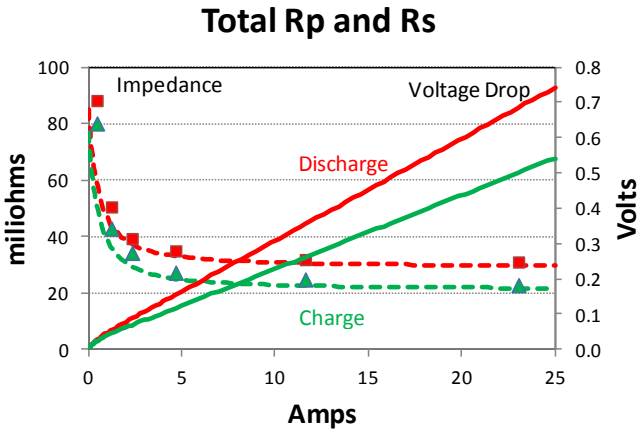

Figure 2 Total Impedance as a Function of Current at mid SOC using data scaled to 20 deg C to compensate for self-heating

The pulse test depicted in Figure 3 and 4 at different temperatures is a charge and discharge cycle with periodic high rate and low rate discharge. Results of the pulse test were used to determine parameter values associated with R_s and R_p, as well as the value of C_p which is currently modeled as a constant value 3 kFarads by matching step values and discharge voltage slopes from test data and model outputs. High rate test data superimposed on a plot of the model output as shown in Figure 5 was used to calibrate thermal model heat capacity and thermal impedance of the cell in the test fixture. The corresponding values are a thermal resistance of 8.5 degC/Watt and a heat capacity of 120 J/degC.

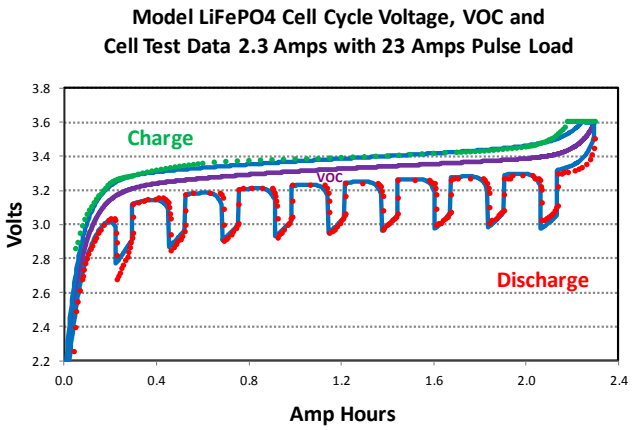

Figure 3 10 C Pulse Test Cycle at 25 deg C
Data points derived from [2] and solid curves from model

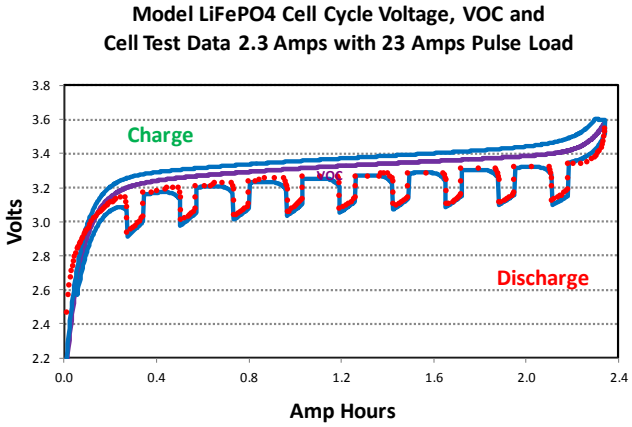

Figure 4 10 C Pulse Test Cycle at 60 deg C.
Data points derived from [2] and solid curves from model

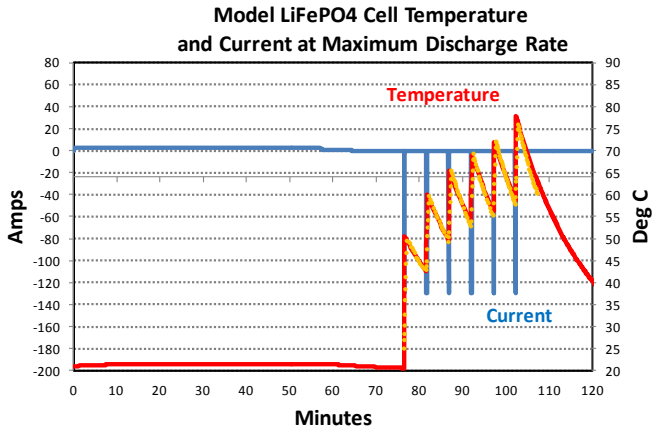

Figure 5 130 Amp Test Cycle with Temperature
Data points derived from [2] and solid curves from model

The measured voltage drop across V_p is across a parallel RC circuit with a time constant on the order of 1 minute and a corresponding value of C_p of approximately 3000F. The resulting component characteristics are depicted in Figures 6a, 6b, and 6c. Compared with the reference unity value at 20 deg C the temperature coefficient causes an eight fold increase in the impedance of the cell at -20C and a decrease to about 60% at +60 deg C as indicated in [13] as well as increasing voltage drops shown in low temperature data from other sources. Some data such as in [2] also indicates reduced cell capacity at very low temperatures however Figure 12 in [14] indicates that the nominal open circuit voltage V_n changes only slightly as a function of temperature.

The model does not specifically include hysteresis as a separate component or two different OCV curves, however energy stored in the smaller capacitor can reproduce what other researchers refer to as hysteresis. Since the impedance components are non-linear and diode like at low current levels, the hysteresis like energy storage can persist for a fairly long time in the model output.

The impedance elements are also functions of SOC with an SOC factor of close to 1 at V_b close to 0 therefore mid SOC and increasing values at high and low SOC. This value is also a function of current direction and is therefore different when charging and discharging the cell with different parameters for R_s and R_p.

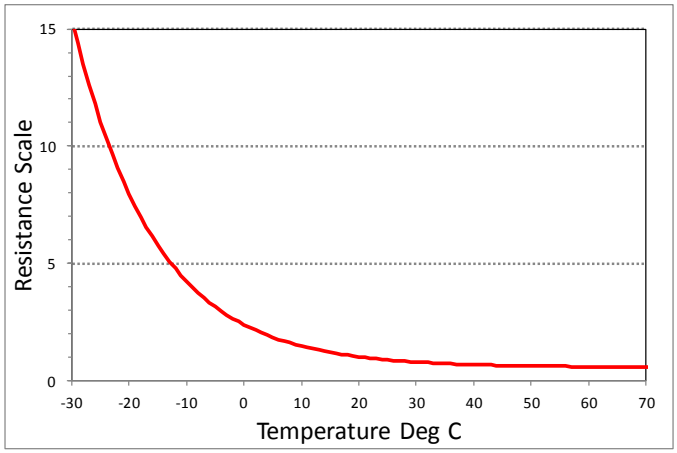

Figure 6a Impedance Temperature Scale Factor with 20 deg C Base

(8) $F(T)= K_n*Exp(K_t*T)+K_m$

(9) $F(T)=1.82*Exp(-0.07*T)+0.56$

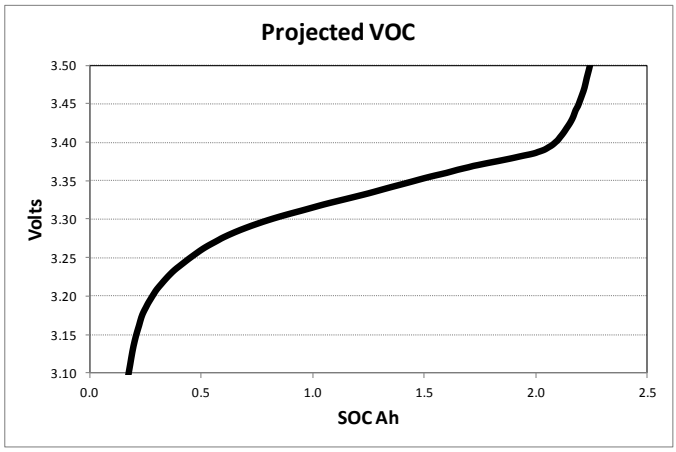

Figure 6b Open Circuit Voltage from Average of Projections

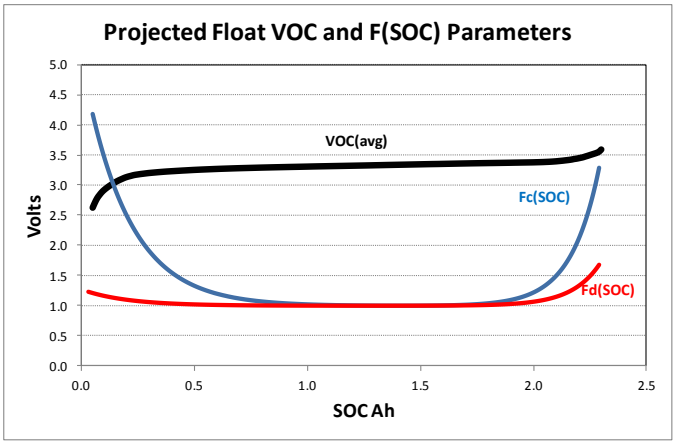

Figure 6c Average Pulse Impedance Scale Factors and V_f

(10) $F(V_b)=(1+(K_{c0}$ or $K_{d0})*Exp((K_{x0}-V_b)*K_{e0}))*(1+(K_{c1}$ or $K_{d1})*Exp((V_b-K_{x1})*K_{e1}))$ where
$K_{c0s}=1.5$, $K_{d0s}=0.1$, $K_{x0s}=-0.097$, $K_{e0s}=75$, $K_{c1s}=0.5$, $K_{d1s}=0.15$, $K_{x1s}=0.035$, $K_{e1s}=120$, $K_{c0p}=0$, $K_{d0p}=0.4$, $K_{x0p}=-0.104$, $K_{e0p}=30$, $K_{c1p}=0.5$, $K_{d1p}=0$, $K_{x1p}=0.035$, $K_{e1p}=45$

Open Circuit Float Voltage Component Parameters

The OCV related components can be projected by running an impedance sub-model over a range of current levels and averaging the resulting OCV estimates. The impedance parameters are corrected by finding a set of OCV solutions that converge towards a common solution. The slope of the curve near mid SOC corresponds to the maximum capacitance as shown in Figure 7a. The sum of Vn and Vb is a linear plot and the voltage controlled voltage source components VCVS0 VCVS1 and VCVS2 add the nonlinear parts of the plot at high and low SOC. These are a polynomial sum and two exponential functions in equation 12. The capacitance is found from the projections based on test data with voltage drops from the impedance sub-model subtracted. The equivalent capacitance of Cb and the three VCVS components is the slope found from numerical differentiation.

Capacitance plots based on data points and the model are plotted as a function of V_f in Figure 7b and as a function of SOC in Figure 7c. The capacitance peak of C_b=52 kFarads corresponding to the minimum slope of the projected V_f plot is at SOC of 1.6 amp hours and V_n=3.355 volts float voltage. Figure 8a and 8b show the model output for one continuous 10C rate charge and discharge cycle including temperature while Figure 9 shows the model output compared to NASA data[1]. The model run starts with charge so the SOC and voltage conditions transition around the loop clockwise starting in the lower left corner of the SOC vs voltage plot.

(11) $V_f=Vn+Vb+Vpoly+Exp1+Exp2$

(12) $V_f=3.355+V_b+k_3*V_b\text{^}3+k_5*V_b\text{^}5+ k_{g0}*Exp(-V_b*km_0)+k_{g1}*Exp(V_b*km_1)$

where
$k_3=35$, $k_5=2000$, $k_{g0}=9.4E\text{-}11$, $km_0=210$, $k_{g1}=1.2E\text{-}5$, $km_1=200$

(13) $V_b=3600*(SOC-1.6)/C_b$

(14) $C_{eq}=I\Delta t/\Delta V$ Farads

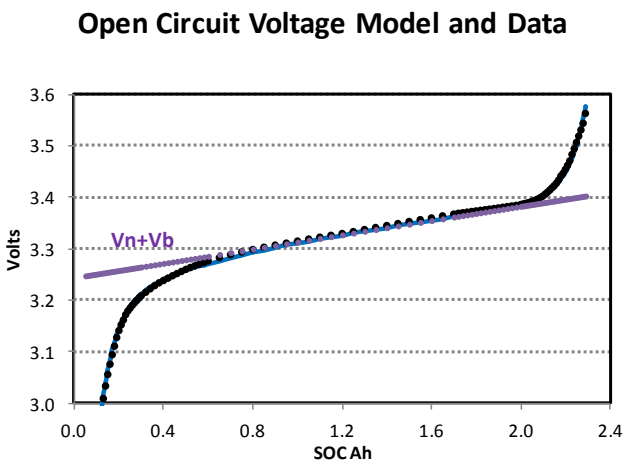

Figure 7a Float Voltage using sum of Nominal Voltage V_n , Bulk Capacitor Voltage V_b and VCVS components as a function of SOC.

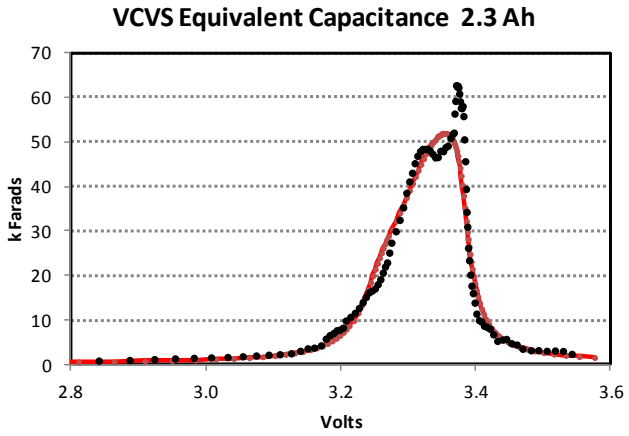

Figure 7b Net Equivalent OCV Capacitance as a function of V_f with points from average projected voc using equation 15 and solid curves from model

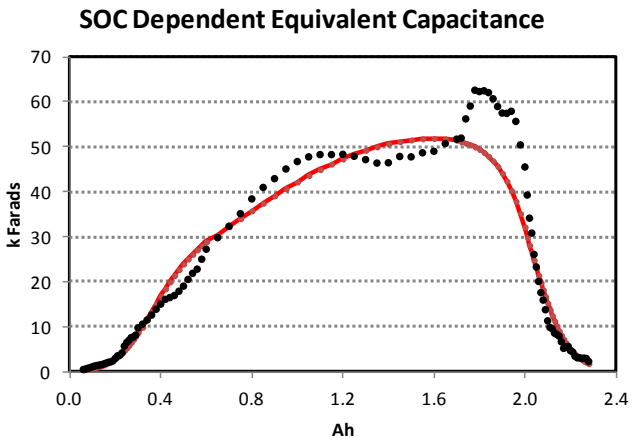

Figure 7c Net Equivalent OCV Capacitance as a Function of SOC with points from average projected voc using equation 15 and solid curves from model

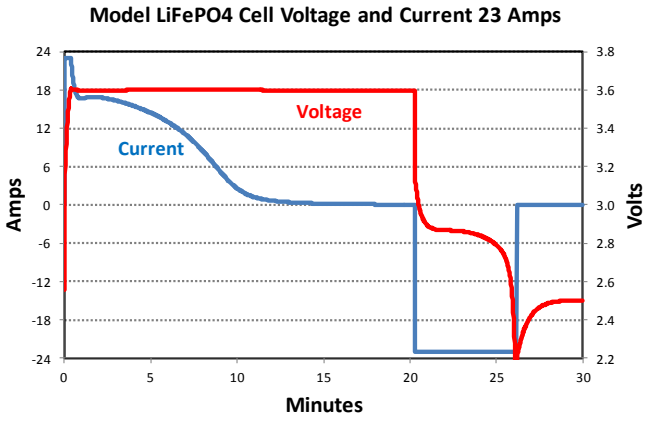

Figure 8a 10C Model Cycle

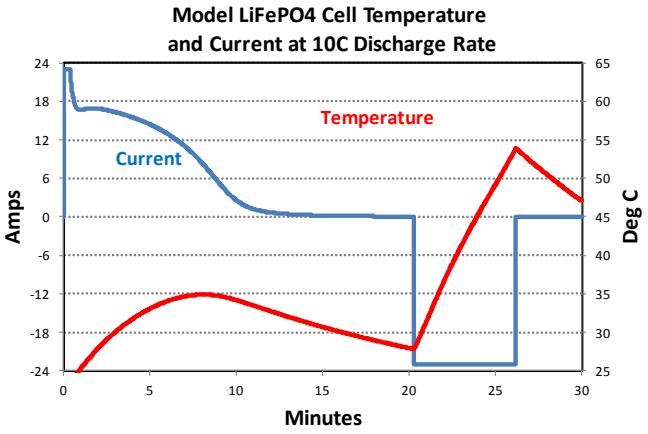

Figure 8b 10C Test Cycle Temperature Projection

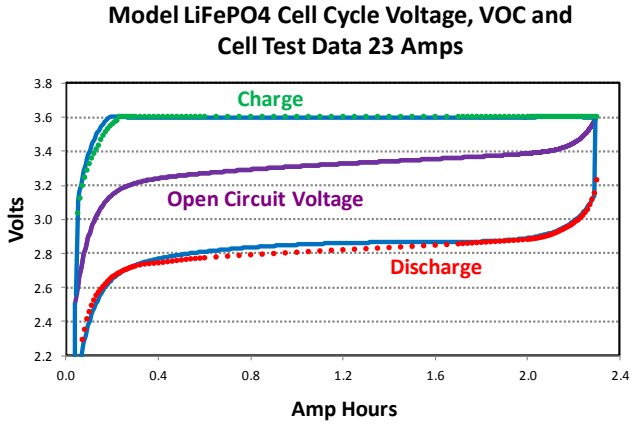

Figure 9 Model and Test Data Cycle as a Function of SOC Data points derived from [1] and solid curves from model

List of Model Variables and Parameters

V_t : Terminal voltage
I_L : Load current
R_L : Cell load resistance
R_s : Series resistor R_s or AC impedance of cell
R_p : Resistor in parallel RC circuit.
C_p : Capacitor in parallel RC circuit
VOC or OCV : open circuit voltage
SOC : State of Charge in amp hours.
V_f : Float open circuit voltage = OCV after $V(C_p) \rightarrow 0$
C_{eq} : Capacitance equivalent to circuit associated with V_f
V_{c0} : Polynomial VCVS term of V_f
V_{c1} : Exponential VCVS term of V_f at high SOC
V_{c2} : Exponential VCVS term of V_f at high SOC
V_n : Nominal cell voltage
C_b : Bulk capacitance of cell at mid SOC and $V_f=V_n$
V_b : Voltage across C_b
T : Temperature in degrees C
t : Time in seconds
F(I), F_s(I), F_p(I) : Component of R_s or R_p Function of I_L
F(I), F_s(I), F_p(I) : Component of R_s or R_p Function of T
F(I), F_s(I), F_p(I) : Component of R_s or R_p Function of V_b
R_{bs} : Base resistance of series resistor R_s
R_{bd} : Additional base resistance of R_s when discharging
R_{bp} : Base resistance of parallel resistor R_p
K_{gs} : Gain coefficient of R_s(I)
K_{gp} : Gain coefficient of R_p(I)
K_{ys} : Offset coefficient of R_s(I)
K_{yp} : Offset coefficient of R_p(I)
K_{zs} : Power coefficient of R_s(I)
K_{zp} : Power coefficient of R_p(I)
K_m : Minimum gain at high temperature of R(T)
K_n : Gain coefficient of resistance temperature compensation
K_t: Exponent coefficient of resistance temp compensation
K_{c0s} : Gain coefficient of R_s(Vb) at low SOC when charging
K_{c1s} : Gain coefficient of R_s(Vb) at high SOC when charging
K_{c0p} : Gain coefficient of R_p(Vb) at low SOC when charging
K_{c1p} : Gain coefficient of R_p(Vb) at high SOC when charging
K_{d0s} : Gain coefficient of R_s(Vb) at low SOC when discharging
K_{d1s}: Gain coefficient of R_s(Vb) at high SOC when discharging
K_{d0p}: Gain coefficient of R_p(Vb) at low SOC when discharging
K_{d1p}: Gain coefficient of R_p(V_b) at high SOC when discharging
K_{e0s}: Exponent coefficient of R_s(V_b) at low SOC
K_{e1s} : Exponent coefficient of R_s(V_b) at high SOC
K_{e0p} : Exponent coefficient of R_p(V_b) at low SOC
K_{e1p} : Exponent coefficient of R_p(V_b) at high SOC
K_{x0s} : Offset coefficient of R_s(V_b) at low SOC
K_{x1s} : Offset coefficient of R_s(V_b) at high SOC
K_{x0p} : Offset coefficient of R_p(V_b) at low SOC
K_{x1p} : Offset coefficient of R_p(V_b) at high SOC
k_3 : Cubic gain of polynomial V_f term
k_5 : Fifth order gain of polynomial V_f term
k_{g0} : Gain coefficient of low SOC exponential term
k_{m0} : Multiplier coefficient of low SOC exponential term
k_{g1} : Gain coefficient of high SOC exponential term
k_{m0} : Multiplier coefficient of high SOC exponential term

Conclusions and Future Work

A spreadsheet based electrical component cell model with typical component values indicated in Figure 10 was developed for the ANR26650M1A lithium iron phosphate cell using published NASA test data. The model reproduces the NASA continuous charge and discharge, interval and pulsed data over a range of temperatures. This model could be converted into a model for use in a simulation tool such as PSpice in order to model a system using many cells and other electrical components such as charge control circuitry and loads. Such a model could project temperatures and voltages in a battery system that may include cell parameter variations and heat transfer variations because of different cell locations in a battery system. Such models may help support system designs or be used as battery fuel gauge applications to estimate remaining state of charge using voltage current and temperature measurements. Models for other types of cells and possibly other energy storage and conversion devices such as ultracapacitors and fuel cells could also be developed.

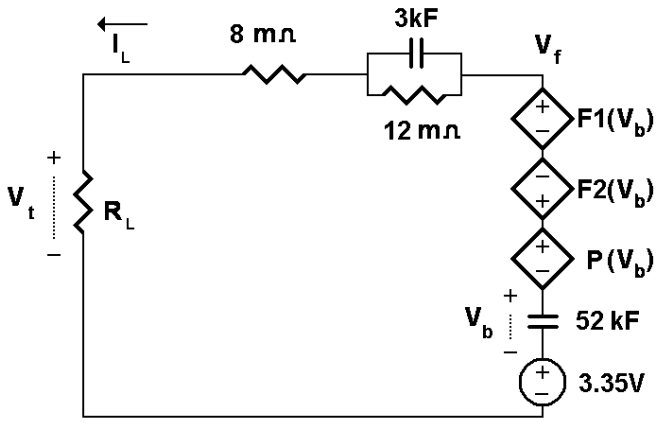

Figure 10 LiFePO4 Cell Model with Typical Element Values

References

[1] C. M. Reid, "Lithium Iron Phosphate Cell Performance Evaluations for Lunar Extravehicular Activities", 10th Electrochemical Power Sources R+D Symposium, Williamsburg, VA, 20-23 Aug, 2007

[2] J. Jeevarajan, B. Strangways and T. Nelson, "Performance and Safety Evaluation of High Rate 18650 Lithium Phosphate Cells", NASA Battery Workshop, November, 2009

[3] E. Prada, D. Di Domenico, Y. Creff, J. Bernard, V.Sauvant-Moynot, F. Huet, "Simplified Electrochemical and Thermal Model of LiFePO4-Graphite Li-Ion Batteries for Fast Charge Applications", Journal of The Electrochemical Society 159, 9 (2012) A1508-A1519

[4] B.M. Huhman, D.A. Wetz, B. Shrestha, P.M. Novak, "Characterization of High Power Battery Cells and Analysis of Battery Module Cooling for Shipboard Pulsed Load Management", Proceedings of ASNE Day 2013, 21-22 Feb. 2013.

[5] D. A. Wetz, B. Shrestha, and P. M. Novak, "Cycling of Electrochemical Energy Storage Devices at Elevated Rates", Proceedings of the 14th DEPS Symposium, http://www.deps.org/.

[6] B.M. Huhman, J.M. Neri and D.A. Wetz, "Design of a Battery Intermediate Storage System for Rep-Rated Pulsed Power Loads", IEEE Electric Ship Technology Symposium Proceedings, April 2013

[7] Mo-Yuen Chow, Srdjan Lukic, Lei Wang, Arvind Govindaraj,"Research Report on A123 Battery Modeling",*www.adac.ncsu.edu/.../**Research**%20Repot%20on%20**A123**%20Battery%*

[8] Robyn Jackey, Michael Saginaw, Pravesh Sanghvi, and Javier Gazzarri, Tarun Huria and Massimo Ceraolo, "Battery Model Parameter Estimation Using a Layered Technique: An Example Using a Lithium Iron Phosphate Cell", SAE International 2013-01-1547

[9] Garo Yessayan, Dipesh D. Patel, Ziyad M. Salameh, "Large Prismatic Lithium Iron Phosphate Battery Cell Model Using PSCAD", Journal of Power and Energy Engineering, 2014, 2, 21-26

[10] Z. Salameh, M. Casacca, and W. Lynch, "A Mathematical Model for Lead-Acid Batteries", IEEE Trans. Energy Conversion, Vol.7, No.1 pp. 93-98 March 1992.

[11] W. A. Lynch and Z. Salameh, "Electrical Component Model for a Nickel-Cadmium Electric Vehicle Traction Battery", Presented at the IEEE Power Engineering Society 2006 PES General Meeting, Montréal, Québec Canada, June 18-22, 2006.

[12] W. Lynch and Z. Salameh, "Realistic Electric Vehicle Battery Evaluation", IEEE Trans. Energy Conversion, Vol.12, No.4, 1997.

[13] Michael Wixom, Suresh Mani, Chuanjing Xu, Biying Huang, Greg Less and Chris Silkowski T/J Technologies, Inc. Ann Arbor, MI, "Lithium Iron Phosphate Applications in Space Power Batteries", https://batteryworkshop.msfc.nasa.gov/presentations/LiIronPhos_Appl_Space_Pwr_Batt_MWixom.pdf

[14] A123 Systems, Inc. "Cylindrical Battery Pack Design, Validation, and Assembly Guide" Document #:493005-001E, February, 2013 http://assets.buya123batteries.com/images/a123/Battery_Pack_Design_Guide_Rev_07.pdf

Biographies

Dr. William A. Lynch Has 26 years of experimental and theoretical R&D experience in the areas of Current Collector/Brush Technology, Energy Storage Device Characterization, Power Electronic Electric Machinery Drive Systems, and Photovoltaic Systems. His graduate degree research focused on development of an Electric Vehicle Battery Evaluation Laboratory Facility and Photovoltaic System Design. He received his BSc, MSc and Doctorate degrees in Electrical Engineering from the University of Massachusetts Lowell in 1987, 1991, and 1997. He participated in Solar Race events including Sunrayce, the World Solar Challenge, and the American Tour De Sol. He has co-authored 32 research papers and DON reports and is a co-inventor on 12 U.S. Navy patents.

Dr. Neal Sondergaard is a senior scientist at BMT Syntek Technologies. He retired from NSWCCD with 29 years experience in R+D including sliding electric contacts(brushes), Tribology, MHD, superconductivity and electric power production, generation, conversion, machinery and distribution and Propulsion System Modeling. He received his B.A. in Chemistry from Marist College, his M.Sc. and Ph.D. in Physical Chemistry from Brown University and was a Post Doctoral Fellow at the Johns Hopkins University. He is a member of Sigma Xi Scientific Research Society, ASNE American Society of Naval Engineers and IEEE. He has co-authored 89 research papers and DON reports and has 10 patents and disclosures.